Magneto-Structural Characterization of Metallocene-Bridged Nitronyl Nitroxide Diradicals by X-Ray, Magnetic Measurements, Solid-state NMR Spectroscopy, and Ab Initio Calculations

Christian Sporer,[b] Henrike Heise,[c] Klaus Wurst,[b] Daniel Ruiz-Molina,[a] Holger Kopacka,[b] Peter Jaitner,*[b] Frank Köhler,*[c] Juan J. Novoa,*[d] and Jaume Veciana*[a]

Abstract: Crystallization of ferrocene and ruthenocene substituted in the 1- and 1′-positions by two nitronyl nitroxide radicals gave the new crystal phases β-**1** (besides the known phase α-**1**), α-**2**, and β-**2** whose structures were determined by X-ray analysis. In β-**1** the radical moieties adopt *transoid* positions, whereas two different *cisoid* conformations are adopted by α-**2** and β-**2**. These conformations result from inter- and intramolecular hydrogen bonds, respectively. All compounds experience antiferromagnetic interactions, and J/k_B values up to −7 K have been found by fitting the experimental magnetic susceptibilities to a modified Bleaney–Bowers equation. The solid diradicals α-**1**, β-**1**, α-**2**, and β-**2** as well as the ferrocene **3**, which was substituted by a unique nitronyl nitroxide, were investigated by ^{13}C and ^{1}H NMR spectroscopy with magic angle spinning. The carbon signals cover a range of 2000 ppm, and are well resolved such that the structure could be confirmed. Conversion of the signal shifts into spin densities disclosed the mechanisms by which spin delocalization from the nitronyl nitroxide substituents to the metallocene core occurs. The spin density distribution in α-**1**, β-**1**, and **3** was also predicted by DFT calculations. There is good agreement between the experimental and theoretical trends of the spin delocalization. The magnetic interactions were discussed in the light of intramolecular spin transfer and its dependence on geometric constraints, demonstrating that the 1,1′-metallocenylene bridge is not a robust magnetic coupler.

Keywords: antiferromagnetic interactions · diradicals · metallocenes · NMR spectroscopy · X-ray analysis

Introduction

The search for ferromagnetic couplers with the aim of obtaining high-spin organic compounds has attracted great interest.[1] One of the potential candidates to realize such high-spin macromolecules is the *m*-phenylene coupler, which has been successfully demonstrated to ferromagnetically couple carbenes[2] as well as triarylmethyl,[3] nitrogen-centered,[4] and nitroxide radicals.[5] The main limitation on increasing the number of aligned spins with *m*-phenylene couplers comes from spin defects and/or bond distortions, mostly due to steric congestion, which have been shown to affect exchange coupling in organic polyradicals.[6] To overcome such problems, other approaches have been used such as the use of π-conjugated linear polymers bearing pendant radical groups[7] or the use of diamagnetic metal ions as ferromagnetic couplers.[8]

Metallocenes are excellent candidates for promoting magnetic interactions between pure organic radicals, not only because of their rich chemistry but also because they are electroactive species whose oxidation state can be controlled

[a] Dr. D. Ruiz-Molina, Prof. J. Veciana
Institut de Ciència de Materials de Barcelona (CSIC)
Campus Universitari de Bellaterra, 08193-Cerdanyola (Spain)
Fax: (+34) 93-5805729
E-mail: vecianaj@icmab.es

[b] C. Sporer, Dr. K. Wurst, Dr. H. Kopacka, Prof. P. Jaitner
Institut für Allgemeine Anorganische und Theoretische Chemie
Universität Innsbruck, 6020, Innrain 52a (Austria)
Fax: (43) 512-507-2934
E-mail: Peter.Jaitner@uibk.ac.at

[c] Dr. H. Heise, Prof. F. Köhler
Anorganisch-chemisches Institut
Technische Universität München 85747 Garching (Germany)
Fax: (+49) 89-2891-3762
E-mail: f.h.koehler@lrz.tu-muenchen.de

[d] Prof. J. J. Novoa
Departament de Química Física and CER Química Teòrica
Facultat de Química, Universitat de Barcelona, Av. Diagonal 647
08028 Barcelona (Spain)
Fax: (+34) 93-402-1231
E-mail: novoa@qf.ub.es

Supporting information for this article is available on the WWW under http://www.chemeurj.org/ or from the author.

 DOI: 10.1002/chem.200305349 © 2004 Wiley-VCH Verlag GmbH & Co. KGaA, Weinheim

chemically and electrochemically, and, most often, the cationic oxidation products are open-shell compounds. However, although such complexes have been successfully used as building blocks for molecular solids that promote intermolecular magnetic exchange interactions,[9] their use as intramolecular magnetic couplers is unprecedented. Recently, we reported a novel family of compounds consisting of two purely organic radicals connected by a 1,1′-metallocenylene bridge. The particular structure of the ferrocene-bridged perchlorotriphenylmethyl diradical **A** allows a non-negligible spin density on the ferrocene moiety, making the ferromagnetic coupling between the two organic radical units feasible.[10] Moreover, the location of both radical units far away from each other avoids any possibility of having intramolecular hydrogen bond interactions and, consequently, a significant direct through-space magnetic interaction.

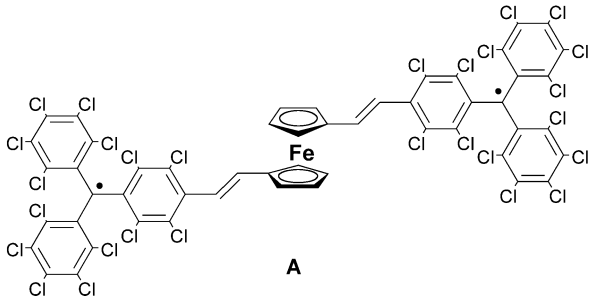

A

The synthesis and properties of metallocene-substituted nitronyl nitroxide diradicals **1** and **2** were also previously described, although the role of the metallocene unit as a magnetic coupler in these compounds was not clearly established.[11] In that study, the spin density on the metallocene units linked to the α-carbon atom of the nitronyl nitroxide radicals was found to be very small. This was because the singly occupied molecular orbital (SOMO) of each nitronyl nitroxide subunit has a node at the α-carbon atom and, therefore, spin density on the metallocene is induced by spin polarization rather than being transmitted directly. Moreover, the X-ray structure found for compound **1**, which from now on will be referred to as the α phase, α-**1**, showed that the two substituents on the cyclopentadienyl (Cp) rings adopt a *cisoid* conformation instead of the *transoid* conformation that would be expected for 1,1′-disubstituted metallocenes bearing conjugated substituents.[12] The *cisoid* conformation is caused by the formation of an intramolecular hydrogen bond between one methyl group of a radical subunit and one of the two N–O groups of the other radical subunit. Such a *cisoid* conformation enables through-space magnetic interaction between the two radical subunits along with the classical spin polarization mechanism through the σ bonds of the metallocene unit. Similar results were found for diradical β-**2**,[11] which was crystallized from Et_2O/*n*-hexane, although at that time no crystals suitable for X-ray structure analysis were obtained.

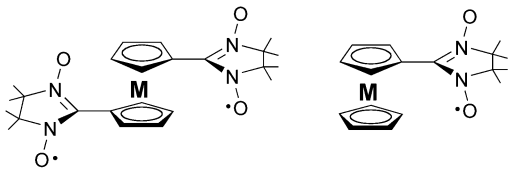

1 M=Fe
2 M=Ru

3 M=Fe

For the above-mentioned reasons, and to fully understand the role of the metallocene unit as a magnetic coupler in metallocene-bridged nitronyl nitroxide diradicals, additional studies were highly desirable. The interest in such studies has increased because metallocene-bridged nitronyl nitroxide diradicals have been used successfully as multicoordinating ligands to obtain transition-metal complexes with unconventional magnetic behavior.[13] In the present work, a comprehensive magneto-structural study of different polymorphic forms of the diradicals **1** and **2** by means of X-ray analysis, magnetic measurements, solid-state NMR spectroscopy, and ab initio calculations is reported.

Results and Discussion

Solid-state structures: Crystallization of compound **1** from MeOH afforded the new crystal phase β-**1**, which crystallizes in the monoclinic $P2_1/n$ space group. The structure together with the crystal packing of diradical β-**1** are shown in Figure 1. General crystallographic data are summarized in Table 1, and selected bond lengths and angles are given in Table 2.

The relevant conformational features of β-**1** are: a) the asymmetric unit consists of half a molecule with the iron atom located at an inversion center, b) the average Fe–C (2.048 Å) and the Fe–Cp (1.676 Å) lengths are those expected for a substituted ferrocene, and c) the imidazoline rings are twisted relative to their adjacent Cp rings with a dihedral angle between the mean planes of both rings of $\varphi = +13.4°$ and $-13.4°$. The opposite signs of both angles are due to the inversion center.

However, the most important feature in the structure of β-**1** is the lack of intramolecular hydrogen bonds that would force the molecule to adopt a *cisoid* conformation, as previously observed for the α-**1** phase.[11] On the contrary, the two Cp rings adopt a *transoid* conformation characteristic of 1,1′-disubstituted metallocenes bearing conjugated substituents. Therefore, the crystal packing of diradical β-**1** seems to be determined by weak intermolecular C–H···O–N hydrogen bonds.[14] The molecules are actually paired and form chains by means of two complementary C–H···O–N bonds between one methyl group of one radical subunit and one of the two N–O groups of the other. The chains are also linked by additional weak C–H···O–N hydrogen bonds.

© 2004 Wiley-VCH Verlag GmbH & Co. KGaA, Weinheim

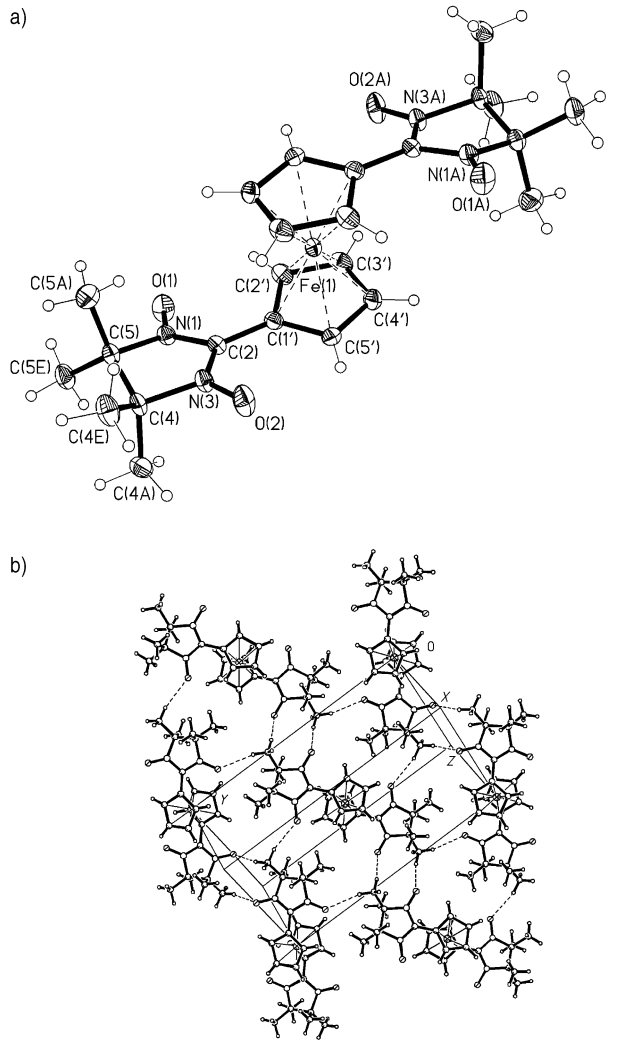

Figure 1. a) Molecular conformation and atomic numbering scheme of β-**1** in the crystal. b) View of the crystal packing of β-**1**.

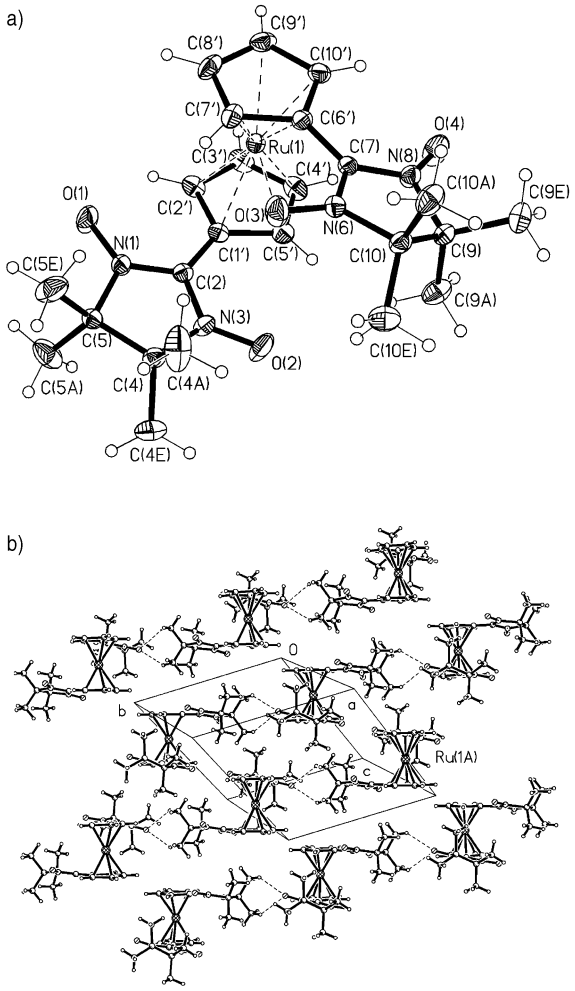

Figure 2. a) Molecular conformation and atomic numbering scheme of α-**2** in the crystal. b) View of the crystal packing of α-**2.**

The α-phase of compound **2**, α-**2**, crystallizes from MeOH in the *P* space group. The molecular structure together with the crystal packing of diradical α-**2** are shown in Figure 2. General crystallographic data are summarized in Table 1 and selected bond lengths and angles are given in Table 3.

Two main conformational features should be emphasized. First, the twist angles between the imidazoline and Cp rings are $\varphi = -11.5°$ and $-12.6°$ and, second, the two substituents on the Cp rings adopt a *cisoid* conformation, as previously observed for α-**1**, also due to the formation of an intramolecular hydrogen bond between one methyl group of one radical subunit and one of the two N−O groups of the other, [H(C(4A))···O(3)−N(6); d(H(C(4A))···O(3)) = 2.60 Å]. The *cisoid* conformation adopted by this radical means that oxygen atoms O2 and O3 are separated by 4.34 Å. The crystal packing of diradical α-**2** seems to be determined by the arrangement of the molecules forming chains along the *b*-axis because of weak hydrogen bonds between the radical oxygen O4 and both methyl groups on the C5 atom [d(H(C(5A′))···O(4)) = 2.49 Å and d(H(C(5E′))···O(4)) = 2.43 Å] of neighboring diradicals. Only weak hydrogen bonds exist between molecules of a given chain and/or adjacent chains. There are further short intermolecular contacts between different radical units [d(O(3)···O(3′)) = 4.13 Å and d(O(1)···O(3′)) = 4.04 Å]. The low symmetry of the molecule is associated with one imidazoline ring being puckered, while the other is flat. This is discussed further in the NMR section.

The β-phase of compound **2** crystallizes from Et_2O/*n*-hexane in the chiral $P3_121$ space group. The asymmetric unit consists of half a molecule with the ruthenium atom located on a twofold rotation axis, thus both radical subunits have equal bond lengths and angles. The molecular structure together with the crystal packing of diradical β-**2** are shown in Figure 3. General crystallographic data are summarized in Table 1, and selected bond lengths and angles are given in Table 4.

In the case of β-**2**, the twist angle between the imidazoline and the Cp rings is $\varphi = +0.8°$. Moreover, the relative arrangement of the two substituents on the Cp rings also adopts a *cisoid* conformation due to the formation of intramolecular hydrogen bonds between one methyl group of

 © 2004 Wiley-VCH Verlag GmbH & Co. KGaA, Weinheim

Table 1. Crystal data and structure refinements for β-**1**, α-**2**, and β-**2**.

	β-**1**	α-**2**	β-**2**
molecular formula	$C_{24}H_{32}FeN_4O_4$	$C_{24}H_{32}N_4O_4Ru$	$C_{24}H_{32}N_4O_4Ru$
formula weight	496.39	541.61	541.61
radiation	$Mo_{K\alpha}$ ($\lambda = 0.71073$ Å)	$Mo_{K\alpha}$ ($\lambda = 0.71073$ Å)	MoKα ($\lambda = 0.71073$ Å)
crystal system	monoclinic	triclinic	trigonal
space group	$P2_1/n$	$P\bar{1}$	$P3_121$
a [Å]	7.074(1)	10.179(2)	12.546(6)
b [Å]	16.806(2)	11.081(2)	12.546(6)
c [Å]	9.867(2)	12.876(2)	13.757(7)
α [°]	90	107.33(1)	90
β [°]	94.71(1)	100.59(1)	90
γ [°]	90	112.69(1)	120
V [Å^3]	1169.1(3)	1203.3(4)	1875.3(16)
Z	*2*	*2*	*3*
temperature [K]	213(2)	218(2)	213(2)
ρ_{calcd} [g cm^{-3}]	1.410	1.495	1.439
μ [mm^{-1}]	0.683	0.689	0.663
$F(000)$	524	560	840
color, habit	green plate	blue plate	blue plate
crystal size [mm^3]	0.9×0.4×0.1	0.3×0.2×0.16	0.25×0.25×0.15
θ, range [°]	3.13–23.50	2.84–23.50	3.25–24.49
reflections collected	2089	3730	2821
independent reflections	1718 [$R_{int} = 0.0244$]	3504 [$R_{int} = 0.0201$]	1585 [$R_{int} = 0.0255$]
reflections $I > 2\sigma(I)$	1468	3179	1482
goodness-of-fit on F^2	1.058	1.029	1.027
final R indices	[$I > 2\ \sigma(I)$]		
R_1	0.0282	0.0261	0.0248
wR_2	0.0664	0.0613	0.0578
R indices (all data)			
R_1	0.0372	0.0311	0.0289
wR_2	0.0727	0.0638	0.0593
extinction coefficient	0.0113(17)	0.0076(6)	
largest diff. peak and hole [e Å^{-3}]	0.281 and −0.238	0.330 and −0.346	0.312 and −0.379
absolute structure parameter (Flack)			−0.03(5)

Table 2. Selected bond lengths [Å], angles [°], and intermolecular contacts for β-**1**.

O(1)−N(1)	1.280(2)	torsion Cp-Cp: 180°
O(2)−N(3)	1.284(2)	dihedral twist angle φ Cp-ONCNO: +/−13.4°
N(1)−C(2)	1.351(3)	torsion angle ONCNO-CMe_2-CMe_2: −/+18°
N(3)−C(2)	1.345(3)	O(1)−O(2A); O(2)−O(1A): 6.84 Å
C(1′)−C(2)	1.446(3)	intermolecular contacts:
O(1)-N(1)-C(2)	126.0(2)	O(1)−H(C5E′); O(1′)−H(C5E): 2.52 Å
O(2)-N(3)-C(2)	126.3(2)	O(1)−C(5E′); O(1′)−C(5E): 3.45 Å
N(1)-C(2)-N(3)	108.8(2)	(1)−O(1)′: 3.98 Å
N(1)-C(2)-C(1′)	125.2(2)	N(1)-O(1)-O(1′); N(1′)-O(1′)-O(1): 104°
N(3)-C(2)-C(1′)	126.0(2)	

one radical subunit and one of the two N−O groups of the other [H(C5AA)···O(2)−N(3); d(O(2)···H(C5AA) = 2.47 Å], resulting in short distances between the two radical oxygen atoms O(2) and O(2A) of 3.43 Å. Intermolecular hydrogen bonds between hydrogen atoms of both Cp rings and both radical subunits of adjacent molecules lead to a helical chain structure along the c axis, where single molecules are twisted by 120° relative to each other [d(H(C(3′)···O(1)) = d(H(C(3′)···O(1′)) = 2.46 Å]. The shortest contacts between radical subunits of different molecules are between adjacent chains [d(O(2)−N(1′)) = 4.80 Å].

Solid-state magnetic properties: Variable-temperature magnetic susceptibility data of compounds α-**1**, β-**1**, α-**2**, and β-**2** were measured on a SQUID susceptometer over the temperature range 2–300 K with an applied external field of 1 kG. As an example, the χT versus T plot of compound α-**2** and the corresponding fit of the experimental data to the modified Bleaney–Bowers equation, which describes the magnetic behavior of a dimer of radicals that interact weakly with its neighbors, are depicted in Figure 4.

At high temperatures (100–300 K) compounds α-**1**, β-**1**, α-**2**, and β-**2** exhibit a constant value of χT of 0.75, 0.76, 0.74, and 0.75 emu K mol^{-1}, respectively, which in each case is close to the expected value for two uncorrelated electrons. By contrast, at low temperatures, the value of χT decreases in all four cases, suggesting that the dominant magnetic interactions are antiferromagnetic. Table 5 shows the intramolecular (intradimer) magnetic exchange coupling constants, J_1/k_B, and the intermolecular (interdimer) magnetic exchange coupling constant, J_2/k_B, values obtained from fitting the data to the Bleaney–Bowers equation ($H = -2\,JS_1 \cdot S_2$) shown in Equation (1), modified to take into account weak intermolecular interactions in the molecular field approximation by Equation (2),[15] where χ is the experimental molar paramagnetic susceptibility, χ_{dimer} the molar paramagnetic susceptibility expected for magnetically isolated dimers, T the temperature, k_B the Boltzman constant, and z the number of neighboring dimers that interact magnetically with each dimer. The resulting intramolecular exchange constants show that the ground states of all compounds are singlets with thermally accessible triplet states.

$$\chi_{dimer} = \frac{0.5}{T\left(1 + \frac{1}{3}\exp\left[\frac{-2J_1}{k_B T}\right]\right)} \quad (1)$$

$$\chi T = \frac{\chi_{dimer} T}{1 - \left[\frac{4zJ_2}{3k_B}\right]\chi_{dimer}} \quad (2)$$

© 2004 Wiley-VCH Verlag GmbH & Co. KGaA, Weinheim

Table 3. Selected bond lengths [Å], angles [°], and intermolecular contacts for α-**2.**

O(1)–N(1)	1.281(3)	O(2)–N(3)	1.283(3)
O(3)–N(6)	1.281(3)	O(4)–N(8)	1.275(3)
N(1)–C(2)	1.346(4)	N(3)–C(2)	1.345(4)
N(6)–C(7)	1.345(4)	N(8)–C(7)	1.346(4)
C(1′)–C(2)	1.448(4)	C(6′)–C(7)	1.455(4)
O(1)-N(1)-C(2)	125.8(2)	O(2)-N(3)-C(2)	125.8(2)
O(3)-N(6)-C(7)	126.1(2)	O(4)-N(8)-C(7)	126.4(2)
N(1)-C(2)-N(2)	108.8(2)	N(1)-C(2)-C(1′)	125.0(2)
N(3)-C(2)-C(1′)	126.2(3)	N(6)-C(7)-N(8)	108.6(2)
N(6)-C(7)-C(6′)	126.5(2)	N(8)-C(7)-C(6′)	125.0(2)

torsion Cp–Cp: 70°
dihedral twist angle φ Cp-O(1)NCNO(2): −11.5°
torsion angle O(1)NCNO(2)–CMe_2–CMe_2: +7.2°
dihedral twist angle φ
Cp–O(3)NCNO(4): −12.6°
torsion angle O(3)NCNO(4)–CMe_2–CMe_2: −15.1°
O(3)–H(C4A): 2.60 Å; O(3)–C(4A): 3.40 Å
O(2)–O(3): 4.34 Å
intermolecular contacts :
O(4)–H(C5A′): 2.49 Å; O(4)–C(5A′): 3.31 Å;
O(4)–H(C5E′): 2.43 Å; O(4)–C(5E′): 3.22 Å
O3–O3′: 4.13 Å; O1–O3′: 4.04 Å

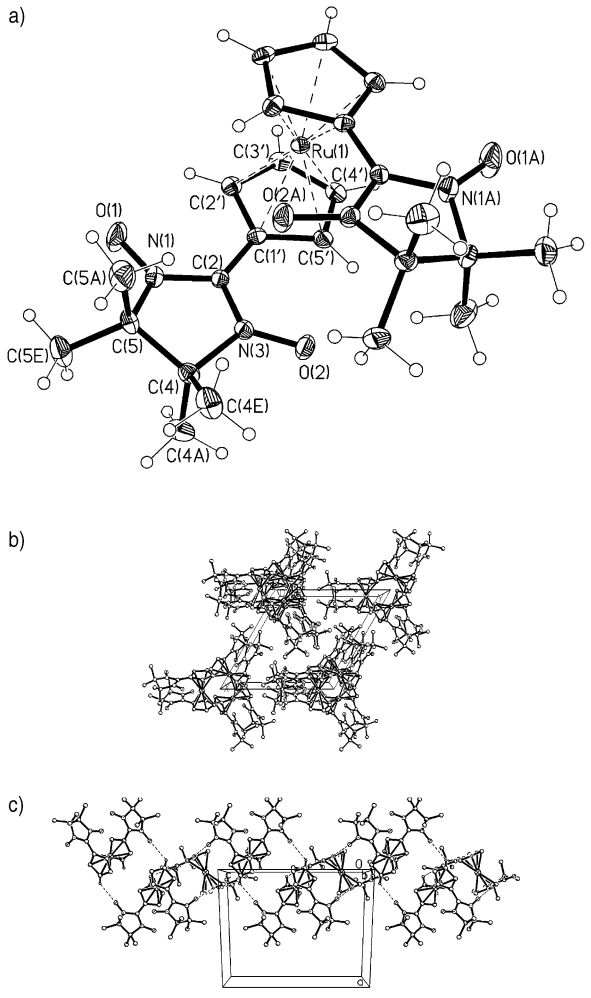

Figure 3. a) Molecular conformation and atomic numbering scheme of β-**2** in the crystal. b) View of the crystal packing of β-**2**. c) View of the 3_1 helical chain structure along the *c* axis.

Table 4. Selected bond lengths [Å], angles [°], and intermolecular contacts for β-**2**.

O(1)–N(1)	1.284(4)	O(2)–N(3)	1.284(4)
N(1)–C(2)	1.358(4)	N(3)–C(2)	1.344(5)
C(1′)–C(2)	1.455(5)	O(1)-N(1)-C(2)	125.9(3)
O(2)-N(3)-C(2)	126.1(3)	N(1)-C(2)-N(3)	108.1(3)
N(1)-C(2)-C(1′)	125.6(3)	N(3)-C(2)-C(1′)	126.3(3)

torsion Cp-Cp: 57°
dihedral twist angle φ Cp-ONCNO: +0.8°
torsion angle ONCNO–CMe_2–CMe_2: −17.4°
O2–H(C5AA): 2.47 Å; O2–C5AA: 3.43 Å
O2–O2A: 3.88 Å
intrachain contacts :
O1–O1′: 5.45 Å
O1–H(C3″); O1′–H(C3′): 2.46 Å
interchain contacts O2-N1′: 4.80 Å

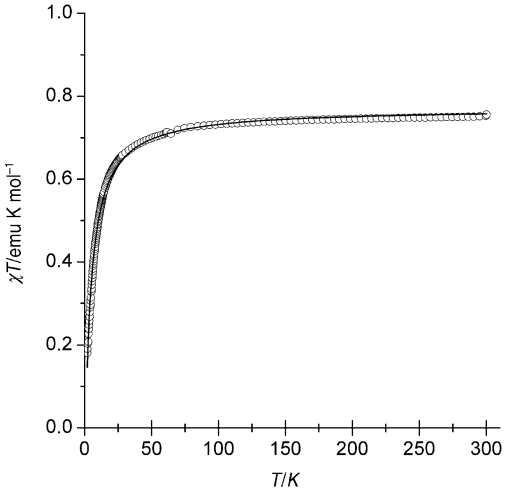

Figure 4. Temperature dependence of the product of molar paramagnetic susceptibility, χ, and temperature, *T*, of phase α-**2**. The solid line represents the fit of experimental data to Equation (2) (see text).

Table 5. Summary of intra- (J_1/k_B) and intermolecular (J_2/k_B) interactions (in K) obtained by fitting the magnetic susceptibility data to Equation (2) that describes the magnetic behavior of diradicals taking into account intermolecular interactions of each dimer with z neighboring dimers in the molecular field approximation.

	J_1/k_B	$z{\cdot}J_2/k_B$
α-**1**	−2.5	−2.5
β-**1**	−5.6	−2.5
α-**2**	−2.5	−4.0
β-**2**	−7.0	−4.0

This result is particularly interesting in the case of β-**1**, since the fit of the paramagnetic susceptibility data to Equation (2) yields a J_1/k_B value of −5.6 K, although in this diradical there is no direct through-space interaction between the two radical units thanks to its *transoid* conformation. Therefore, in β-**1** the intramolecular antiferromagnetic interaction must take place exclusively through the skeleton by a spin polarization mechanism. This result is in contrast with that obtained previously for the ferrocene-bridged perchlorotriphenylmethyl diradical **A**, which also has a *transoid* conformation but exhibits an intramolecular ferromagnetic cou-

 © 2004 Wiley-VCH Verlag GmbH & Co. KGaA, Weinheim

pling. This fact is a clear indication that the nature and topology of radical units play a key role in the transmission of the magnetic coupling through the metallocene coupler. Thus, the observed differences in the intramolecular magnetic interactions of β-**1** and the diradical **A** originate from two main sources. First, only little spin density is located on the metallocene unit of diradical β-**1**, because the relevant MO has a node at carbon 2 of the nitronyl nitroxide radicals, while this does not apply for the ferrocene-bridged perchlorotriphenylmethyl diradical. Second, the twist angles are $\varphi = +13.4°$ and $-13.4°$, which may change the magnetic ground state from triplet to singlet (see below). From the above considerations it can be concluded that the 1,1′-metallocenylene bridge can act as a ferromagnetic coupler when radical units with proper topologies are connected to them. Nevertheless, this bridge is not a robust magnetic coupler since small distortions or improper topologies may revert the metallocene to the expected spin multiplicity of its ground states.

Another noteworthy result is the different intramolecular antiferromagnetic interactions of the two phases of the ruthenocene-bridged diradicals **2**. For β-**2** it is almost three times larger than for α-**2** (Table 5). This must be ascribed to the different conformations found by X-ray analysis (Figure 2 and 3). It substantiates previous results on the ferrocene-bridged diradical α-**1**, for which the interaction in frozen solution is almost twelve times larger than in the crystal, a fact that had been attributed tentatively to conformational changes.[11]

How do conformational changes affect intramolecular magnetic exchange interactions in metallocene-based nitronyl nitroxide diradicals? Considering that the magnetic interaction in compounds **1** and **2** can take place either by a classical spin polarization mechanism across the Cp rings and the metal of the metallocene unit, or by a through-space interaction between the two radical units, or by a combination of both mechanisms, two main conformational features may play a critical role in the intramolecular magnetic interactions. These are: 1) the twist angle φ between the imidazoline radical and its adjacent Cp ring and 2) the relative position of the two ONCNO fragments of the diradical, where most of the spin density is located. Concerning the first of these, variations of φ may be reflected in the strength of the intramolecular magnetic exchange coupling simply by disturbing the spin polarization mechanism. In fact, φ has been shown to dramatically affect exchange couplings in organic diradicals;[6] according to ab initio calculations on *m*-phenylene coupled diradicals, a large φ between the radical-bearing groups and the central phenyl ring may switch off conjugation and hence decrease the strength of the magnetic interaction and even reverse the magnetic ground state from triplet to singlet.[6a] Such structure–property relationships have been observed experimentally for *m*-phenylene-type[16] and trimethylenemethane-type diradicals.[17] Keeping the above considerations in mind, compounds α-**2** and β-**2** were analyzed. Thus, in α-**2**, the twist angles between the imidazoline and Cp rings are $\varphi = -11°$ and $-12°$, whereas in β-**2** both angles φ are close to zero, thereby promoting a stronger magnetic exchange interaction between the radical units. The second contribution to the large discrepancy of the J_1/k_B values found for compounds α-**2** and β-**2** are different N–O···O–N contacts, expected to be most important for a through-space interaction between the two radical units. The analysis of the geometry showed that the O···O length for α-**2** is 4.34 Å, whereas the same length for β-**2** is only 3.88 Å. Although the presence of short N–O···O–N contacts is not unequivocally indicative of dominant antiferromagnetic interactions,[18] the shorter O···O length of β-**2** points to a more efficient through-space interaction between the two radical units.

Solid-state NMR spectroscopy and spin densities: ^{13}C and ^{1}H MAS NMR spectra were obtained for the compounds α-**1**, β-**1**, α-**2**, β-**2**, and **3**. A particularly well-resolved example is reproduced in Figure 5. It shows two sets of carbon signals, one for each of the crystallographically different subunits of α-**1**. The shift ranges of the signals of the magnetically active nuclei correspond to what has been found previously.[19] Thus, the signals of methyl groups in axial position of the puckered imidazole ring appear at $\delta = 1000$–1200 ppm and those of the equatorial methyl groups at $\delta = 350$–650 ppm, while the ring carbon signals of the nitronyl nitroxide core appear between $\delta = -600$ and -800 ppm. The bridging ferrocene of α-**1** displays carbon signals whose shifts are similar to those of various phenyl groups bonded to C2 of the nitronyl nitroxide.[18] The signals of C1′ and C6′ fall into the shift range of equatorial methyl carbon atoms. Yet they can be identified by their line widths, which are smaller than those of the adjacent signals, because C1′ and C6′ are more remote from the NO spin sources, and thus dipolar relaxation is less efficient. Some carbon signals of ferrocene were hidden under the background signal of the

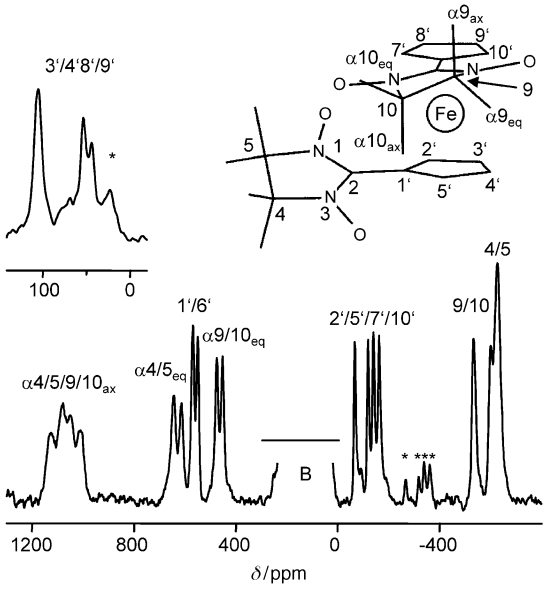

Figure 5. ^{13}C MAS NMR spectrum of α-**1** (309.6 K, spinning rate 15 kHz). Asterisks: spinning sidebands; B: probe head signal; inset: expanded range after background suppression. For more detailed signal assignment see text.

© 2004 Wiley-VCH Verlag GmbH & Co. KGaA, Weinheim

probe head; they were disclosed by background suppression (Figure 5, inset).

The more detailed signal assignment relies on the distribution of the unpaired spin density in the molecule, because the NMR contact shift, δ_T^{con}, at the temperature T is proportional to the spin density, $\rho(N)$, at the nucleus N [Eq. (3)] ,[20] where μ_0 is the vacuum permeability, g_{av} the mean g factor, μ_B the Bohr magneton, a_0 the Bohr radius, S the electron spin quantum number and $\rho(N)$ is obtained in atomic units.

$$\rho(N) = \frac{9k_B T}{\mu_0 g_2^{av} \mu_2^B a_0 (S+1)} \delta_{con}^T \quad (3)$$

The experimental signal shifts are converted into paramagnetic shifts, δ_{para}^T, as described in the Experimental Section. In general, δ_{para}^T values are composed of contact and dipolar shift contributions. However, as the g-factor anisotropy of organic radicals is small, the dipolar shifts are negligible in this case and one can approximate $\delta_{para}^T \sim \delta_{con}^T$.

Qualitatively, there are two pathways for releasing spin density from a π-faced spin source into a conjugated Cp ligand (Figure 6a). When the spin source Y is bonded directly to Cp, a large amount of spin will be transferred to C2′/5′ and little to C1′ and C3′/4′. Hence, we expect large positive signal shifts for C2′/5′ and negative signal shifts (induced by polarization) for C1′ and C3′/4′. This is true where Y is a paramagnetic transition-metal fragment, and is the case for the diradical **A**.[21] By contrast, when the spin source Y is separated from Cp by a nucleus X as in Figure 6b, the signs of the signal shifts are inverted. The latter case applies for the nitronyl nitroxide derivatives of this work where X is the C2 (or C6) of the nitronyl nitroxide to which two spin sources (the NO groups) are bonded. As will be shown below, there is generally little spin density on C3′/4′, and, therefore, its sign may switch from positive to negative. On this basis the pairs C2′/5′ and C7′/10′ have been distinguished from C3′/4′ and C8′/9′, respectively.

The signals of the two Cp rings of α-**1** can be distinguished in the crystal structure:[11] The twist angle, φ (see Figure 6b), between the nitronyl nitroxide and the Cp rings of one subunit is 7°, while for the second one it is 24°. As shown in substituted *m*-phenylene diradicals,[16] a smaller twist angle entails better conjugation and hence more spin

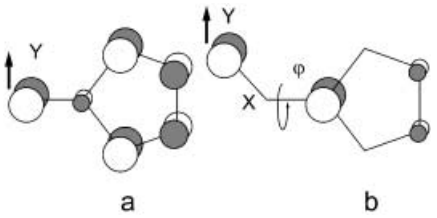

Figure 6. Qualitative MO results after attaching π-faced spin sources Y to cyclopentadienyl separated by a) one bond, b) two bonds by means of nucleus X.

density is induced in the Cp ring. Therefore, of the two signals near $\delta = 600$ ppm, the more shifted one is assigned to the ligand with $\varphi = 7°$. The same applies to all other Cp carbon resonance, while the distinction of C2′ and 5′, C3′ and 4′, $C\alpha 4_{ax}$ and 5_{ax}, $C\alpha 4_{eq}$ and 5_{eq} as well as similar pairs follows the spin densities obtained from DFT calculations (see below). Table 6 collects the ^{13}C contact shifts of α-**1** as well as those of all other compounds.

Table 6. ^{13}C and ^{1}H MAS NMR contact shifts[a] of metallocenes substituted by α-nitronyl nitroxides.

Nucleus and position[b]	α-**1**	β-**1**	α-**2**	β-**2**	**3**
$C\alpha 4_{ax}$	1150	1268	1004	1069[d]	1121
$C\alpha 5_{ax}$	1103	1181	1004	1158[d]	1121
$C\alpha 4_{eq}$	647	396	803[d]	424[d]	551
$C\alpha 5_{eq}$	615	380	861[d]	399[d]	502
C4	−722	−627	−816	−656	−708
C5	−722	−612	−816	−600	−708
C1′	507.6	535.1	461.6	465.6	440.4
C2′	−246.3	−157.1	−176.7	−156.7	−149.9
C3′	−14.6	−12.2	−22.5	−8.0	−38.4
C4′	38.8	2.9	20.9	107.3	63.1
C5′	−222.6	−119.8	−176.5	−156.7	−100.3
C_5H_5					27.5
$C\alpha 9_{ax}$	1070		1014[c][d]		
$C\alpha 10_{ax}$	1027		1045[d]		
$C\alpha 9_{eq}$	471		601[d]		
$C\alpha 10_{eq}$	448		564[d]		
C9	−624		−638[e]		
C10	−694		−716[e]		
C6′	486.2		461.6		
C7′	−200.5		−176.7		
C8′	38.8		−22.5		
C9′	**−24.6**		**20.9**		
C10′	−147.0		−176.5		
$H\beta 4,5,9,10_{ax}$	−16.8	−13.8	−17.0	−16.8	−16.6
$H\beta 4,5,9,10_{eq}$	−14.1	−13.8	−17.0	−12.3	−11.5
Hα2′, 5′, 7′, 10′	14.6	16.3	18.0	19.3	13.7
Hα3′, 4′, 8′, 9′	−3.5	−0.1	−0.2	2.9	−3.4
C_5H_5					1.3

[a] Paramagnetic shifts δ at 298 K. [b] For numbering see Figures 5–7. [c] Shoulder of the signal at $\delta =$ 1004 ppm. [d] Distinction of the pairs of $C\alpha_{ax}$ and of $C\alpha_{eq}$ follows from Equation. (2) as described in the text and listed in Table SI1 in the Supporting Information. [e] Distinction between C9/10 not clear.

Other remarkable features emerge in the ^{13}C MAS NMR spectrum of the ruthenium derivative α-**2** (Figure 7). There is only one set of signals for the Cp rings of the different subunits which is in accord with the almost equal twist angles ($\varphi = -11°$ and $-12°$) of the Cps relative to the nitronyl nitroxide moieties. However, for the latter there are two sets of signals, and the signals of two out of four equatorial methyl groups have unusually large shifts (about $\delta =$

 © 2004 Wiley-VCH Verlag GmbH & Co. KGaA, Weinheim

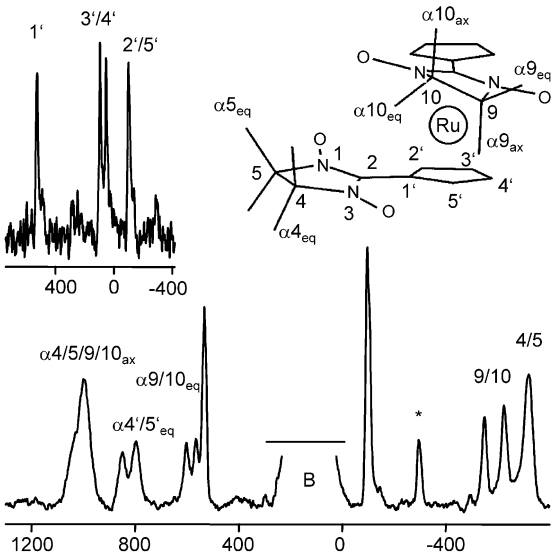

Figure 7. ^{13}C MAS NMR spectrum of α-**2** (309.6 K, spinning rate 15 kHz). Asterisk: spinning sideband; B: probe head signal; inset: expanded range after background suppression.

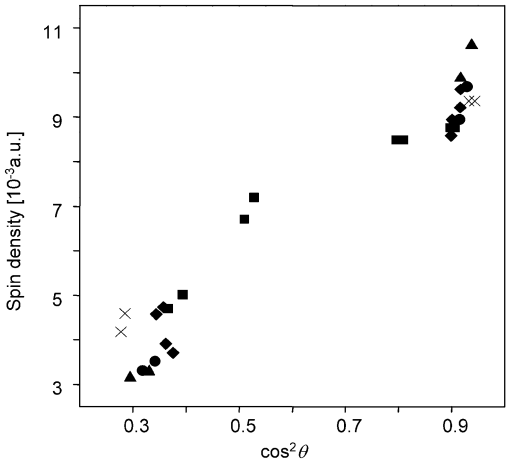

Figure 8. Nitronyl nitroxides: experimental spin densities versus orientation of the methyl groups relative to the spin-containing NO groups. See Equation (2) and text for details. ◆ = α-**1**, ▲ = β-**1**, ■ = α-**2**, ● = β-**2**, × = **3**).

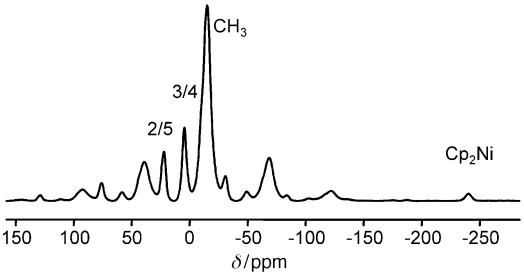

Figure 9. ^{1}H MAS NMR spectrum of α-**2** (309.6 K, spinning rate 15 kHz). Nonassigned signals are spinning sidebands; Cp_2Ni is the internal temperature standard. For numbering see Figure 7.

800 ppm), whereas the two remaining ones stay in the known range at about $\delta = 600$ ppm. It follows that the two nitronyl nitroxide moieties must be rather different and that two equatorial methyl groups must interact more efficiently with the spin-containing p orbital at the adjacent nitrogen atom than the others. This interaction is known as hyperconjugation and may be described empirically by Equation (4), where δ_0 and B are constants and θ is the dihedral angle between a C–CH_3 bond and the direction of the p orbital of the adjacent nitrogen atom.

$$\delta^{con} = \delta_0 + B\cos^2\theta \quad (4)$$

The p orbital can be approximated by the normal to the plane, which contains that nitrogen atom (Table S1 in the Supporting Information). The large signal shifts of $C\alpha_{eq}$ in α-**2** correspond to unusually small angles θ. This in turn means that the nitronyl nitroxide is almost flat rather than puckered, as it is usual for this kind of radical. The flat conformation adopted by the imidazoline ring is in agreement with the X-ray results.

Equation (4) is applicable generally and the correlation of $\cos^2\theta$ with the signal shifts of the methyl carbon atoms of α-**1**, β-**1**, α-**2**, β-**2**, and **3** is illustrated in Figure 8. The geometry of different nitronyl nitroxide cores changes only a little so that in Figure 8 the axial and the equatorial methyl groups appear in the upper right and the lower left part, respectively. An exception is α-**2**, for which $\cos^2\theta$ is close to 0.5. As expected for the flat nitronyl nitroxide ring of α-**2**, the small θ values of the equatorial methyl groups are compensated by dihedral angles of the axial methyl groups that are larger than usual. Therefore, the corresponding $\cos^2\theta$ values appear at 0.8, which is also outside the usual range.

The ^{1}H MAS NMR spectra of α-**1**, β-**1**, α-**2**, β-**2**, and **3** showed much smaller signal shifts. An example is the spectrum of α-**2** in Figure 9 in which two sorts of Cp protons and the methyl protons give rise to separate signals. In addition, axial and equatorial methyl groups could be distinguished for α-**1**, β-**2**, and **3** (Table 6), but further distinction of different ligands in a given compound (e.g. α-**1**) was prevented by large signal widths. Note, however, that the resolution is much better than for the EPR spectra where spin density on the Cp protons could not be detected.[11]

Comparison of NMR results and DFT calculations: To understand in more detail the magnetic interactions in diradicals **1** and **2**, their spin density distributions were calculated by using an ab initio method. These were done using the experimental geometry of the compounds taken from their crystals. All calculations were done using the B3LYP nonlocal exchange-correlation density functional[22] as implemented in the Gaussian98 suite of programs,[23] and the EPR–II basis set.[24] Such a basis set was specifically designed to reproduce the spin population on the nucleus, the important point in the computation of EPR hyperfine coupling constants (hfccs).[25] The atomic spin populations were obtained following the Mulliken population scheme. It should be pointed out here that the computed values for the H atoms have been averaged over all equivalent atoms, to emulate the experimental conditions, where these atoms are freely exchanging (on the rotating methyl groups) or are not easy

© 2004 Wiley-VCH Verlag GmbH & Co. KGaA, Weinheim

to distinguish experimentally (in the case of the H atoms attached to the five-membered rings) because of their small hfcc values. Thus, we should not expect a high accuracy for the spin density on H atoms at these positions.

For comparison with the theoretical spin densities, the NMR contact shifts of Table 6 were converted into spin densities using Equation (3). As can be seen in Table 7, the trends of the experimental spin densities are well reproduced by the DFT calculations. We can say that the relative trends are correct, despite the fact that the quantitative values present sometimes non-negligible differences to the experimental data. In particular, this applies to the Cp rings. Thus, in all compounds, by far the largest amount of (positive) spin density is found on C1′ (and C6′), there is always more negative spin on C2′ than on C5′, and there is very little spin on C3′ and C4′. It is gratifying that, throughout the series of compounds, the spin density on one of the two latter carbon atoms is negative, while on the other one it is positive.

Table 7. Calculated[a] and experimental spin densities[b] on the nucleus of metallocenes substituted by α-nitronyl nitroxides.

Nucleus and position[c]	α-**1**		β-**1**		**3**	
	ρ^{calcd}	ρ^{exp}	ρ^{calcd}[d]	ρ^{exp}	ρ^{calcd}	ρ^{exp}
$C\alpha4_{ax}$	3.95	9.27	3.97	9.92	8.09	9.42
$C\alpha5_{ax}$	4.09	9.67	4.45	10.66	8.60	9.42
$C\alpha4_{eq}$	1.50	3.96[g]	1.10	3.33[h]	1.97	4.22
$C\alpha5_{eq}$	1.50	3.76[g]	1.10	3.20[h]	2.15	4.64
C2	−16.96	[e]	−17.19	[e]	−35.05	[e]
C4	−2.90	−6.07	−2.57	−5.15	−4.60	−5.95
C5	−2.85	−6.07	−2.85	−5.27	−5.50	−5.95
C1′	2.72	4.27	2.97	4.50	7.74	3.70
C2′	−0.52	−2.07	−0.57	−1.32	−1.82	−1.26
C3′	−0.07	−0.12	0.02	0.02	0.02	−0.32
C4′	0.10	0.33	−0.15	−0.10	−0.10	0.53
C5′	−0.95	−1.87	−0.67	−1.01	−2.47	−0.84
C_5H_5					−0.07	0.23
$C\alpha9_{ax}$	4.47	8.99				
$C\alpha10_{ax}$	4.30	8.63				
$C\alpha9_{eq}$	1.90	5.44				
$C\alpha10_{eq}$	1.72	5.17				
C7	−17.14	[e]				
C9	−3.20	−5.83				
C10	−3.12	−5.24				
C6′	3.37	4.09				
C7′	3.95	−1.69				
C8′	0.07	0.33				
C9′	−0.05	−0.21				
C10′	−1.60	−1.24				
$H\beta4,5,9,10_{ax}$[f]	−0.14	−0.14	−0.06	−0.12	−0.11	−0.14
$H\beta4,5,9,10_{eq}$[f]	−0.87	−0.12	0.07	−0.12	−0.16	−0.10
Fe	−9.87	[e]	−10.84	[e]	−13.94	[e]
Hα2′, 5′, 7′, 10′	0.10	0.12	0.15	0.14	0.09	0.12
Hα3′, 4′, 8′, 9′	0.01	−0.03	0.01	0.00	0.01	−0.03
C_5H_5					−0.01	0.01

[a] B3LYP functionals, EPR–II basis set. [b] In atomic units $\times 10^{-3}$. [c] Numbering see Figures 5–7. [d] Mean of slightly different values for the two ligands. [e] Not observed. [f] ρ^{calcd} are mean values of the geometrically fixed protons of four methyl groups. [g,h] Assignment follows from Equation (2) in the Discussion and the data given in Table SI1 in the Supporting Information.

The spin density patterns of the Cp rings confirm that the spin is transferred from the nitronyl nitroxide into the Cp π orbitals. In a metallocene the MOs are composed of varying contributions of the metal orbitals and the (mainly) π orbitals of both Cp ligands. It follows that in the monoradical **3**, where only one Cp is substituted by a nitronyl nitroxide, the unsubstituted Cp must receive spin density as well (Table 7 and Figure 10). For instance, it has been demonstrated that in a bismetallocene, which consists of a paramagnetic cobaltocene coupled to a diamagnetic cobaltocenium ion, considerable spin density appears at the most distant Cp ligand of the diamagnetic sandwich.[26] Likewise, in the case of **3** the spin transfer to the distant Cp is confirmed by the NMR and DFT results (see C_5H_5 in Table 7). As this spin density is small and as the DFT result is the average of five different Cp nuclei, there is a variety of spin signs in Table 7. A similar reasoning applies to the results for the methyl protons, βH. EPR spectroscopy has shown that there is also spin density at the transition metal, for example, at iron and ruthenium in α-**1** and α-**2**, respectively, as well as in β-**1**, in agreement with DFT calculations (Table 7 and Figure 10).[11]

Conclusion

Subtle changes in the framework of hydrogen bonds have a strong impact on the conformations and structure of metallocenes that are substituted by two nitronyl nitroxide radicals. Experimentally these changes can be triggered by different conditions of crystallization. The molecular geometries differ in the twist angle φ between the nitronyl nitroxide and the Cp rings of a given ligand, in the *cisoid* or *transoid* arrangement of the two ligands, and in the puckering of the nitronyl nitroxide rings. The different geometries are reflected in the intramolecular antiferromagnetic interaction, which is large if the diradical adopts a *cisoid conformation* in which the two nitronyl nitroxide moieties are close to each other. Nevertheless, the intramolecular magnetic exchange interactions, J_1/k_B, do not exceed −7 K in any case.

Solid-state NMR spectroscopy and DFT calculations, independently and in good agreement, confirm spin density on the nuclei of the radical subunits. As for the Cp rings, spin is induced in π orbitals through polarization and further transfer occurs across the central iron and ruthenium atoms. Although it can be proven that the spin density on the Cp ring decreases when the twist angle φ increases, φ values up to 12° do not strongly influence the magnetic interaction.

 © 2004 Wiley-VCH Verlag GmbH & Co. KGaA, Weinheim

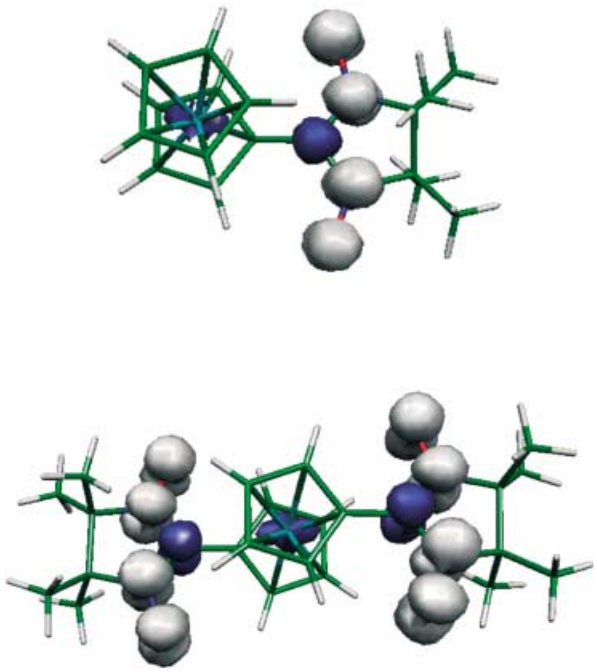

Figure 10. Spin density maps of monoradical **3** (upper) and diradical β-**1** (lower) obtained by DFT calculations. Each map plots the isosurface of 0.05 a.u. It is worth mentioning the presence of spin density on the nuclei of Cp rings (see text) at smaller isosurface values that are not shown here for clarity.

The spin density patterns further indicate whether the respective nitronyl nitroxide ring is puckered or flat.

In principle, 1,1′-metallocenylene bridges can act either as ferro- or antiferromagnetic couplers depending on the nature of the radical units of the diradical. The character of antiferromagnetic coupling shown by the metallocene coupling unit in the nitronyl nitroxide case, opposed to the ferrocoupler behavior found when the radical unit was a triphenylmethyl radical, cannot be ascribed to the lack of planarity of the radical units, relative to the Cp planes, since coplanarity is not found in either radical. The most important difference is the presence of a node in the nitronyl nitroxide case for the SOMO in the atom where the radical is attached to the metallocene unit; a fact not present in the triphenylmethyl radical case. This makes the overlap of the SOMO of the nitronyl nitroxide units with the metallocene orbital very small. However, the presence of such a node does not preclude spin polarization in the Cp ring (using a spin polarization mechanism similar to that found in phenyl substituted nitronyl nitroxide radicals). The data presented here indicates that when such a node exists antiferromagnetic coupling is preferred, although none of the usual qualitative models seems to explain this fact easily.

In summary, the extensive results presented here demonstrate that metallocene is not a robust magnetic coupler for obtaining high-spin organic macromolecules since small distortions or improper topologies of the radical units may change the spin multiplicity of the ground states. For this reason, future work will be focused on the use of metallocene-bridged nitronyl nitroxide polyradicals as new multicoordinating ligands with a view to obtaining transition-metal complexes.

Experimental Section

Compounds **1**, **2**, and **3** were synthesized by reaction of the corresponding metallocene mono- and biscarbaldehydes[27] with 2,3-bis(hydroxyamino)-2,3-dimethylbutane[28]. After oxidation with PbO_2 and chromatographic workup the pure products were obtained in 62, 80, and 64% yield, respectively. Experimental details are available as Supporting Information.

Direct current magnetic susceptibility measurements were carried out on a Quantum Design MPMS SQUID susceptometer with a 55 kG magnet operating in the range of 2–320 K. All measurements were collected at a field of 1 kG. Background correction data were collected from magnetic susceptibility measurements on the sample holder. Diamagnetic corrections estimated from the Pascal contents were applied to all data for the determination of the molar paramagnetic susceptibilities of the compounds.

X-ray data were collected on a Bruker-P4 with a graphite monochromator, and the structures were solved by direct methods using SHELXS-86 and refined by full-matrix least-squares methods on F^2 (SHELXL-93)[29]. CCDC-215329 (α-**2**), CCDC-215330 (β-**1**), and CCDC-215331 (β-**2**) contain the supplementary crystallographic data for this paper. These data can be obtained free of charge via www.ccdc.cam.ac.uk/conts/retrieving.html (or from the Cambridge Crystallographic Data Centre, 12, Union Road, Cambridge CB21EZ, UK; fax: (+44) 1223-336-033; or deposit@ccdc.cam.ac.uk).

The ^{13}C and ^{1}H MAS NMR spectra were recorded with a Bruker MSL 300 spectrometer. The microcrystalline compounds were mixed in a glove box with about 10% of nickelocene which served as internal temperature standard.[30] They were then packed into ZrO_2 rotors of 4 mm diameter and sealed with Kel-F caps. Single pulses of 4 μs duration at repetition rates of 2.5–5 s^{-1} were applied for obtaining the FIDs. Signals hidden under the background signal of the probe head were detected by using the DEPTH pulse sequence.[31] Data handling included reverse linear prediction, exponential multiplication up to the matched filter, and base line correction. The experimental signal shifts, δ_T^{exp}, were determined relative to external adamantane ($\delta(^{13}CH_2)=29.5$, $\delta(^{1}H)=2.0$). The paramagnetic signal shifts, δ_T^{para}, were obtained after subtracting from δ_T^{exp} the signal shifts of corresponding nuclei of diamagnetic reference compounds. Since diamagnetic analogues of α/β-**1**, α/β-**2**, and **3** are not available, we used the NMR data of the precursors of **1** and **2**, whose values are given in the Supporting Information material. The signal shifts of most similar compounds used were: the dihydroprecursor of an α-nitronyl nitroxide documented in reference [18] ($\delta(CH_3)=1.07$, $\delta(CH_3)=20.7$, $\delta(C4/5)=66.3$), formylferrocene[32] ($\delta(H2'/5')=4.81$, $\delta(H3'/4')=4.60$, $\delta(C1')=79.2$, $\delta(C2'/5')=72.6$, $\delta(C3'/4')=68.0$) and 1′, 1′-diacylruthenium[33] ($\delta(H2'/5')=5.09$, $\delta(H3'/4')=4.78$, $\delta(C1')=86.5$, $\delta(C2'/5')=73.1$, $\delta(C3'/4')=75.6$). The sample temperatures lay between 305 and 310 K depending on the rotor spinning rate. The $\delta^{exp}{}_T$ values were converted to the standard temperature 298 K based on the relation $\delta_{\alpha}^{para} 1/T$.

Acknowledgments

This work was supported by grants DGI (Projects MAT2003-04699 and BQU2002-04033-C02-01), CIRIT (Projects 2000SGR 00114 and 2001SGR-0044), Fonds zur Förderung der Wissenschaftlichen Forschung, Vienna (Project P13128), Austrian Federal Ministry of Science (BMWV), Acción Integrada Hispano-Austríaca (HU-2002–0046), and the 3MD Network of the TMR program of the E.U. (contract ERBFMRX CT980181). C. S. thanks the Austrian Federal Ministry of Science for the award of a research scholarship, H. H. and F. H. K. thank the Fonds der Chemischen Industrie for financial support, and J. J. N. thanks CESCA/CEPBA and the CEPBA-IBM Research Institute for allocation of computer time.

© 2004 Wiley-VCH Verlag GmbH & Co. KGaA, Weinheim

[1] For a collection of reviews on high-spin organic molecules see: a) J. Veciana, H. Iwamura, *MRS Bull* **2000**, *36*, 41; b) *Magnetic Properties of Organic Materials* (Ed.: P. M. Lahti), Marcel Dekker, New York, **1999**; c) J. S. Miller, J. A. Epstein, *Angew. Chem.* **1994**, *106,* 399; *Angew. Chem. Int. Ed. Engl.* **1994**, *33, 106*, 385; d) A. Rajca, *Chem. Rev.* **1994**, *94*, 871; e) M. Baumgarten, K. Millen, *Top. Curr. Chem.* **1994**, *164*, 1; f) H. Iwamura, N. Koga, *Acc. Chem. Res.* **1993**, *26*, 346; g) D. A. Dougherty, *Acc. Chem. Res.* **1991**, *24*, 88.

[2] a) K. Matsuda, N. Nakamura, K. Takahashi, K. Inoue, N. Koga, H. Iwamura, *J. Am. Chem. Soc.* **1995**, *117*, 5550; b) N. Nakamura, K. Inoue, H. Iwamura, *Angew. Chem.* **1993**, *105*, 900; *Angew. Chem. Int. Ed. Engl.* **1993**, *32* 872-874.

[3] a) N. Ventosa, D. Ruiz, J. Sedó, X Tomas, C. Rovira, B. Andre, J. Veciana, *Chem. Eur. J.* **1999**, *5*, 3533; b) J. Sedó, N. Ventosa, D. Ruiz-Molina, M. Mas, E. Molins, C. Rovira, J. Veciana, *Angew. Chem.* **1998**, *110,* 344; *Angew. Chem. Int. Ed.* **1998**, *37*, 330; c) D. Ruiz-Molina, J. Veciana, F. Palacio, C. Rovira, *J. Org. Chem.* **1997**, *62*, 12; d) J. Veciana, C. Rovira, N. Ventosa, M. I. Crespo. F. Palacio, *J. Am. Chem. Soc.* **1993**, *115*, 57; e) A. Rajca, S. Rajca, J. Wongsriratanakul, *J. Am. Chem. Soc.* **1999**, *121*, 6308; f) A. Rajca, J. Wongsriratanakul, S. Rajca, R. Cerny, *Angew. Chem.* **1998**, *110*, 1284; *Angew. Chem. Int. Ed.* **1998**, *37*, 1229; g) K. R. Stickley, S. C. Blackstok, *J. Am. Chem. Soc.* **1994**, *116*, 11576.

[4] a) K. Yoshizawa, A. Chano, A. Ito, A. Tanaka, T. Yamabe, H. Fujita, J. Yamauchi, M. Shiro, *J. Am. Chem. Soc.* **1992**, *114*, 5994; b) K. R. Stickley, S. C. Blackstock, *J. Am. Chem. Soc.* **1994**, *116*, 11576; c) R. J. Bushby, D. R. McGill, K. M. Ng, N. J. Taylor, *J. Chem. Soc. Perkin Trans.* **1997**, *2*, 1405.

[5] a) A. Calder, A. R. Forrester, P. G. James, G. R. Luckhurst, *J. Am. Chem. Soc.* **1969**, *91*, 3724; b) K. Mukai, H. Nagai, K. Ishizu, *Bull. Chem. Soc. Jpn.* **1975**, *48*, 2381; c) T. Ishida, H. Iwamura, *J. Am. Chem. Soc.* **1991**, *113*, 4238; d) F. Kanno, K. Inoue, N. Koga, H. Iwamura, *J. Phys. Chem.* **1993**, *97*, 13267.

[6] It is well-documented that large bond torsions in *m*-phenylene-bridged polyradicals result in antiferromagnetic exchange couplings: a) D. A. Shultz, A. K. Boal, G. T. Farmer, *J. Am. Chem. Soc.* **1997**, *119*, 3846; b) S. Fang, M. Lee, D. A. Hrovat, W. T. Borden, *J. Am. Chem. Soc.* **1995**, *117*, 6727; c) J. Fujita, M. Tanaka, H. Suemune, N. Koga, K. Matsuda, H. Iwamura, *J. Am. Chem. Soc.* **1996**, *118*, 9347; d) J. A. Berson, *Acc. Chem. Res.* **1997**, *30*, 238.

[7] a) T. Michinobu, M. Takahashi, E. Tsuchida, H. Nishide, *Chem. Mater.* **1999**, *11*, 1969; b) H. Nishide, M. Miyasaka, E. Tsuchida, *Angew. Chem.* **1998**, *110*, 2497; *Angew. Chem. Int. Ed.* **1998**, *37*, 2400; c) P. J. VanMeurs, R. A. J. Janssen, *J. Org. Chem.* **2000**, *65*, 5712.

[8] a) D. M. Adams, A. L. Rheingold, A. Dei, D. N. Hendrickson, *Angew. Chem.* **1993**, *105*, 434; *Angew. Chem. Int. Ed. Engl.* **1993**, *32*, 391; b) A. Caneschi, A. Dei, D. Gatteschi, *J. Chem. Soc., Chem. Commun.* **1992**, *630*.

[9] See ref. [1c] and references therein.

[10] a) O. Elsner, D. Ruiz-Molina, J. Vidal-Gancedo, C. Rovira, J. Veciana, *Chem. Commun.* **1999**, 579; b) O. Elsner, D. Ruiz-Molina, I. Ratera, J. Vidal-Gancedo, C. Rovira, J. Veciana, *J. Organomet. Chem.* **2001**, *637*, 251.

[11] O. Jürgens, J. Vidal-Gancedo, C. Rovira, K. Wurst, C. Sporer, B. Bildstein, H. Schottenberger, P. Jaitner, J. Veciana, *Inorg. Chem.* **1998**, *37*, 4547.

[12] a) A. J. Moore, P. J. Skabara, M. R. Bryce, A. S. Batsanov, J. A. K. Howard, S. T. Daley, *J. Chem. Soc. Chem., Commun.* **1993**, 413b) F. Gelin, R. P. Thummel, *J. Org. Chem.* **1992**, *57*, 3780.

[13] a) D. Ruiz-Molina, C. Sporer, K. Wurst, P. Jaitner, J. Veciana, *Angew. Chem.* **2000**, *112*, 3842; *Angew. Chem. Int. Ed.* **2000**, *39*, 3688. 36; b) C. Sporer, D. B. Amabilino, D. Ruiz-Molina, K. Wurst, P. Jaitner, J. Veciana, *Chem. Commun.* **2002**, 2342.

[14] M. Deumal, J. Cirujeda, J. Veciana, M. Kinoshita, Y. Hosokoshi, J. J. Novoa, *Chem. Phys. Lett.* **1997**, *265*, 190.

[15] W. E. Hatfield, R. R. Weller, J. W. Hall, *Inorg. Chem.* **1980**, *19*, 3825.

[16] a) F. Kanno, K. Inoue, N. Koga, H. Iwamura, *J. Am. Chem. Soc.* **1993**, *115*, 847; b) J. Fujita, M. Tanaka, H. Suemune, N. Koga, K. Matsuda, H. Iwamura, *J. Am. Chem. Soc.* **1996**, *118*, 9347; c) L. Catalá, J. LeMoigne, N. Kyritsakas, P. Rey, J. J. Novoa, P. Turek, *Chem. Eur. J.* **2001**, *11*, 2466.

[17] D. A. Shultz, A. K. Boal, H. Lee, G. T. Farmer, *J. Org. Chem.* **1999**, *64*, 4386.

[18] a) M. Deumal, J. Cirujeda, J. Veciana, J. J. Novoa, *Chem. Eur. J.* **1999**, *5*, 1631; b) M. Deumal, J. Cirujeda, J. Veciana, J. J. Novoa, *Adv. Mater.* **1998**, *10*, 1461.

[19] H. Heise, F. H. Köhler, F. Mota, J. J. Novoa, J. Veciana, *J. Am. Chem. Soc.* **1999**, *121*, 9659.

[20] F. H. Köhler in *Magnetism: Molecules to Materials. Models and Experiments* (Eds.: J. S. Miller, M. Drillon) Wiley-VCH, Weinheim, **2001**, Chapter 12.

[21] F. H. Köhler, W. A. Geike, P. Hofmann, U. Schubert, P. Stauffert, *Chem. Ber.* **1984**, *117*, 904.

[22] B3LYP is a density functional obtained by taking the three parameter nonlocal exchange funcional of Becke (A. D. Becke, *J. Chem. Phys.* **1993**, *98*, 5648) and the non-local correlation functional of Lee, Yang and Parr (C. Lee, W. Yang, R. G. Parr, *Phys. Rev. B.* **1988**, *37*, 785).

[23] Gaussian 98, Revision A.7, M. J. Frisch, G. W. Trucks, H. B. Schlegel, G. E. Scuseria, M. A. Robb, J. R. Cheeseman, V. G. Zakrzewski, J. A. Montgomery, Jr., R. E. Stratmann, J. C. Burant, S. Dapprich, J. M. Millam, A. D. Daniels, K. N. Kudin, M. C. Strain, O. Farkas, J. Tomasi, V. Barone, M. Cossi, R. Cammi, B. Mennucci, C. Pomelli, C. Adamo, S. Clifford, J. Ochterski, G. A. Petersson, P. Y. Ayala, Q. Cui, K. Morokuma, D. K. Malick, A. D. Rabuck, K. Raghavachari, J. B. Foresman, J. Cioslowski, J. V. Ortiz, A. G. Baboul, B. B. Stefanov, G. Liu, A. Liashenko, P. Piskorz, I. Komaromi, R. Gomperts, R. L. Martin, D. J. Fox, T. Keith, M. A. Al-Laham, C. Y. Peng, A. Nanayakkara, C. Gonzalez, M. Challacombe, P. M. W. Gill, B. Johnson, W. Chen, M. W. Wong, J. L. Andres, M. Head-Gordon, E. S. Replogle, J. A. Pople, Gaussian, Inc., Pittsburgh PA, **1998**.

[24] V. Barone in *Recent Advances in Density Functional Methods, Part I* (Ed.: D. P. Chong), World Scientific Publisher, Singapore **1996**.

[25] This has permitted us to evaluate the confidence of the calculated hfcc values with the experimental ones obtained under isotropic conditions. Those corresponding to the values expected to be found in the absence of any solvent interaction that, therefore mimic the values in gas phase were also evaluated. See: J. Cirujeda, J. Vidal-Gancedo, O. Jürgens, F. Mota, J. J. Novoa, C. Rovira, J. Veciana *J. Am. Chem. Soc.* **2000**, *122*, 11393.

[26] H. Hilbig, F. H. Köhler, *New J. Chem.* **2001**, *25*, 1152.

[27] a) G. G. A. Balavoine , G. Doisneau , T. Fillebeen-Kahn, *J. Organomet. Chem.* **1991**, *412*, 381; b) R. Sanders , U. T. Mueller-Westerhoff, *J. Organomet. Chem.* **1996**, *512*, 219; c) U. T. Mueller-Westerhoff, Z. Yang, G. Ingram, *J. Organomet. Chem.* **1993**, *463*, 163.

[28] a) V. I. Ovcharenko, S. V. Fokin, G. V. Romanenko, I. V. Korobkov, P. Rey, *Russ. Chem. Bull.* **1999**, *48*(8), 1519; b) V. Ovcharenko, S. Fokin, P. Rey, *Mol. Cryst. Liq. Cryst. Sci. Technol. Sect. A* **1999**, *334*, 109; c) C. Hirel, K. E. Vostrikova, J. Pecaut, V. I. Ovcharenko, P. Rey, *Chem. Eur. J.* **2001**, *7*, 2007.

[29] a) G. M. Sheldrick, SHELXS-86 program for crystal structure solutions, Göttingen, **1986**; b) G. M. Sheldrick, SHELXL-93 program for refinement of crystal structures, Göttingen, **1993**.

[30] H. Heise, F. H. Köhler, X. Xie, *J. Magn. Reson.* **2001**, *150*, 198.

[31] D. C. Cory, W. M. Ritchey, *J. Magn. Reson.* **1988**, *80*, 128.

[32] a) M. D. Rausch, A. Siegel, *J. Organomet. Chem.* **1969**, *17*, 117; b) A. A. Koritze, P. V. Petrovskii, A. I. Mokov, I. A. Lutsenko, *J. Organomet. Chem.* **1977**, *136*, 57.

[33] J. Sandström, J. Seita, *Acta Chem. Scand. Ser. B* **1977**, *31*, 86.

Received: July 18, 2003
Revised: October 21, 2003 [F5349]

 © 2004 Wiley-VCH Verlag GmbH & Co. KGaA, Weinheim